

AEROELASTIC STABILITY ASSESSMENT OF AN INDUSTRIAL COMPRESSOR BLADE INCLUDING MISTUNING EFFECTS

Yaoguang Zhai Ronnie Bladh*† Göran Dyverfeldt
Siemens Industrial Turbomachinery AB
SE-612 83 Finspong, Sweden

ABSTRACT

This paper presents a comprehensive investigation into the aeroelastic stability behavior of a transonic front blade in an industrial compressor when operating outside its normal range of service parameters. The evolution of the airfoil's aeroelastic stability in the first flexural mode is studied as the front blade operation progresses towards choked flow conditions.

First, linearized 3D flutter computations representing today's industry standard are performed. The linearized calculations indicate a significant, shock-driven flutter risk at these off-design flow conditions. To further explore the aeroelastic behavior of the rotor and to find a viable solution toward flutter risk elimination, two parallel investigations are undertaken: (i) flow perturbation nonlinearity effects and potential presence of limit-cycle oscillation; and (ii) effects of blade mistuning and flutter mitigation potential of intentional mistuning, including its impact on forced response behavior.

The nonlinear harmonic analyses show that the minimum aerodynamic damping increases rapidly and essentially linearly with blade oscillation amplitude beyond the linear regime. Thus, a state of safe limit-cycle oscillation is predicted for the fully tuned blade. Additionally, it is found that intentional, realizable blade frequency offsets in an alternating pattern efficiently stabilize the blade. Finally, it is verified that alternating mistuning has a beneficial effect versus the inevitable random mistuning also in the forced response.

NOMENCLATURE

1F	First Flexural Mode
AC	Aerodynamic Coupling
CFD	Computational Fluid Dynamics
DOF	Degree(s) of Freedom
EO	Engine Order
HCF	High Cycle Fatigue
IGV	Inlet Guide Vane
IM	Intentional Mistuning
LogDec	Logarithmic Decrement
LP	Loading Parameter
MAC	Modal Assurance Criterion
ND	Nodal Diameter
PS	Pressure Side
RM	Random Mistuning
SC	Structural Coupling
SS	Suction Side
TWM	Traveling Wave Mode
c	chord length
f	first flexural mode eigenfrequency
k	reduced frequency
\mathbf{u}	mode shape vector
v	relative inlet flow velocity
*	complex conjugate transpose

INTRODUCTION

High cycle fatigue in turbomachinery blading stemming from a variety of excitation sources continues to attract the attention of industrial and academic researchers [1–4]. The sources of excitation are more or less obvious. Among the obvious ones

*Address all correspondence to this author at ronnie.bladh@siemens.com.

†ASME member.

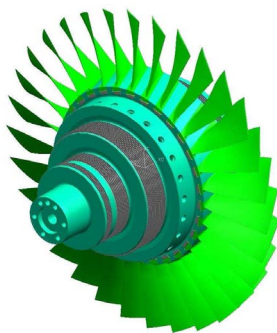


FIGURE 1. 3D VIEW OF THE INVESTIGATED FRONT STAGE COMPRESSOR ROTOR.

one notes the synchronous unsteady flow perturbations due to upstream and downstream vanes (for blades). Numerous studies of synchronous excitation mechanisms of both experimental and numerical character have been published over the past decades [5, 6]. Less obvious are nonsynchronous types of excitation, which may derive from any one or combinations of boundary layer separation, shock-boundary layer interactions, vortex shedding, tip/hub vortices, and rotating stall. With ever-increasing computational power and powerful model reduction techniques at researchers' disposal, numerical modeling and prediction capabilities are emerging also in this extremely challenging field [7, 8]. A third source of HCF damage is self-induced blade excitation known commonly as flutter. Flutter in turbomachinery is an aeroelastic instability in the coupled fluid-structure system consisting of an oscillating blade surrounded by flowing gas. This has also occupied many researchers over the years with varying levels of complexity and detail, ranging from analytical 1D models to nonlinear, time-marched 3D computations with fully coupled fluid-structure models of high spatial resolution [9, 10]. On the positive side, flutter occurrences are rare in conventionally designed blades and vanes under intended operating conditions. On the other hand, the flutter instability mechanism can typically lead to instant blade HCF failure without giving a possibility to react on damage indications during overhauls etc.

The third excitation source — flutter — is the focus of this paper. The overall objective of the presented investigation is to determine the flutter risk for an existing front stage, transonic compressor blade design when operating outside the normal envelope of service parameters. Figure 1 provides a 3D view of the investigated front stage rotor. The numerical investigation into the blade's aeroelastic behavior is first conducted in accordance with today's industry-standard (linear) methodology, and then expanded into studies of nonlinear flow perturbations as well as effects of blade mistuning. To accomplish this, a number of tasks need to be performed as described by the paper's organizational structure below.

First, some basic background to the problem at hand is outlined. This is followed by brief descriptions of employed fluid and structural models together with their fundamental results on which the rest of the analyses rely. For linearized aerodynamic damping calculations it is imperative that the steady state basis about which the unsteady perturbations act is of high quality. Transonic blades require particular attention in this regard since significant portions of the aerodynamic work done on the blade can be expected to stem from shock oscillation.

With above prerequisites in place, the performed harmonic flutter analyses are presented. This section first outlines the general basis for the computations, followed by a presentation of the obtained results utilizing the standard, linear harmonic approach. In the linearized unsteady calculations, a linear relationship between blade vibratory amplitude and the induced unsteady forces is assumed for analytical model simplification and thus solver efficiency purposes. This simplified approach proves to be both efficient and accurate enough as long as the blade vibrates with small amplitudes. For large vibration amplitudes, however, the induced unsteady forces may deviate significantly from those of linearized solutions in both magnitude and phase [11]. Consequently, this section moves on to describe the performed nonlinear harmonic simulations and obtained results. The findings from these analyses are compared, discussed, and explained.

Next, the attention is turned to mistuning and particularly its potential to mitigate flutter. Mistuning refers to the ever-present blade-to-blade deviations in geometry and/or material properties stemming from manufacturing, raw material processes, and wear. Hence, a bladed disk is always a structure with individual blades rather than a cyclic symmetric assembly. The intense research on the subject over the past decades has shown that mistuning may alter drastically the dynamic behavior of bladed disks and blisks, e.g., see [12] and references therein. A topic of particular interest to this investigation is the effects of intentional mistuning, which is typically a deliberate detuning of certain blades in an assembly. The introduction of intentional mistuning has been shown through numerical investigations [13–15] and even in engineering practice [16, 17] to be a practical and effective measure to alleviate flutter. The mistuning section included here describes the outcomes of the performed statistical analyses of mistuned aeroelastic stability with respect to random mistuning with and without intentional mistuning. A brief study of mistuned forced response behavior is also included to complete the investigation.

CASE BACKGROUND

As mentioned previously in the introduction, the key objective of the presented study is to determine the flutter risk for an existing front stage compressor blade design when operating outside the normal envelope of service parameters. The blade operates in the transonic regime at a total-to-total pressure ratio of 1.68 during nominal, full load operation. The investigated blade

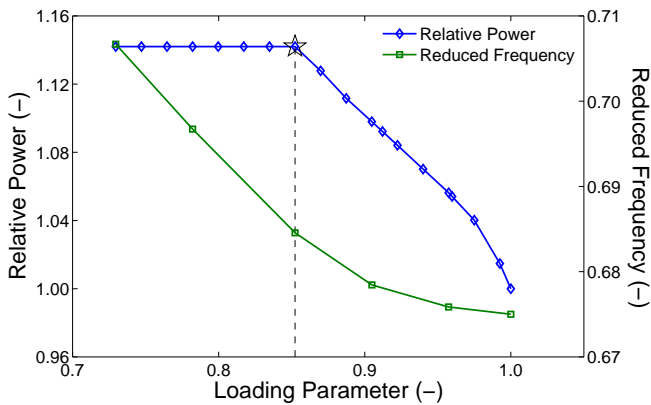


FIGURE 2. EVOLUTION OF ENGINE OUTPUT POWER AND 1F REDUCED FREQUENCY WITH LOADING PARAMETER.

is found in a mid-range industrial gas turbine that is used for both mechanical drive and power generation applications. The engine has a proven track record of reliability and robustness over a wide range of operating parameters, which are here stretched beyond current fleet experience.

Figure 2 depicts schematically the engine relative output power as function of a loading parameter LP. Regrettably, the definition of the parameters in Fig. 2 cannot be disclosed here. The operating point where the relative power and the loading parameter both equal one is here regarded as the nominal case. The aeroelastic investigation presented here looks at loading parameter levels below this nominal condition. One can note from Fig. 2 that the otherwise monotonic increase in relative output power as the loading parameter decreases is controlled to a maximum value at about 1.14 when the loading parameter passes below approximately 0.85 (marked with a dashed line). This is a design integrity-induced power limitation that is independent of the aeroelastic instability phenomenon discussed in this paper.

Moreover, Fig. 2 includes the reduced frequency k as function of the loading parameter, where the reduced frequency is defined according to traditional convention [18]:

$$k = \frac{2\pi fc}{v} \quad (1)$$

Here, f denotes the first flexural mode (1F) eigenfrequency of the blade, c is the chord length, and v is the relative inlet flow velocity. The latter two quantities are taken at 75% span. It is observed in Fig. 2 that reduced frequencies remain essentially the same over the depicted loading range. It is further notable that with reduced frequencies around 0.7 the blade is well above any reduced frequency limits that are traditionally seen as lower design limits to alleviate flutter risks (typically 0.3–0.5). Hence, one would not expect to see classical flutter tendencies for this blade.

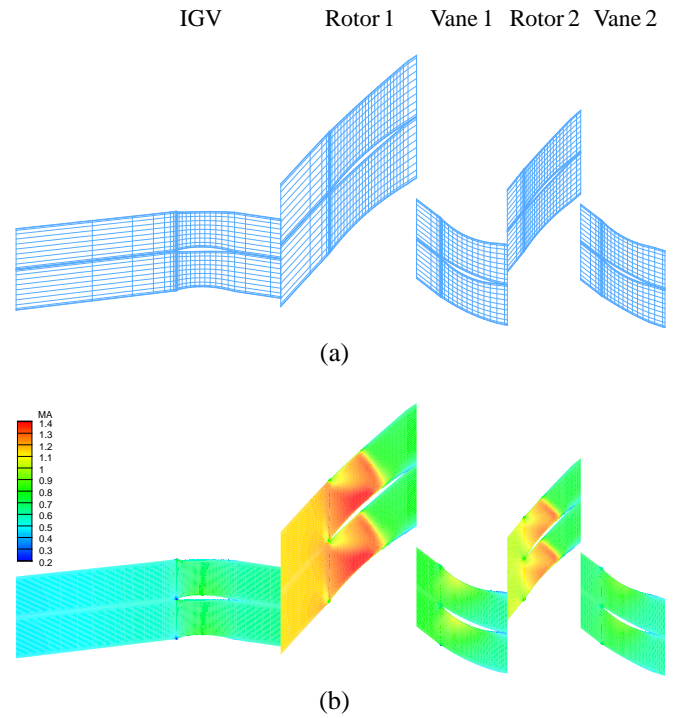


FIGURE 3. MIDSPAN MERIDIONAL VIEW OF THE EMPLOYED 2.5-STAGE CFD GRID WITH EVERY 4th GRID LINE SHOWN (a) AND STEADY STATE RELATIVE MACH NUMBER DISTRIBUTION FOR THE NOMINAL CASE LP=1.0 (b). TWO PASSAGES PER ROW ARE SHOWN FOR PROFILE VISIBILITY.

COMPUTATIONAL MODEL

Flow Simulation Model

The CFD model used in the computations includes the first two and half stages in the compressor, from inlet guide vane to vane 2. The computational grid is a simple H grid and consists of $49 \times 136 \times 46 = 306,544$ cells in the rotor 1 domain and 1,174,334 cells in total for the 2.5-stage model. A midspan meridional view of the employed computational grid is shown in Fig. 3(a). Note in Fig. 3 that two passages per row are shown to make the airfoil profiles visible. Moreover, the computational grid in Fig. 3(a) is coarsened by showing every fourth grid line only in order to give an appreciable view of the employed grid distribution. This grid is the end result of a limited grid convergence study (not presented here) that was carried out to ensure robust, high fidelity steady state results. It should also be mentioned that the rotor tip gaps are included in the model, while the hub leakage beneath the shrouded stators is ignored.

This investigation employs the in-house CFD code TF3D, which solves the unsteady 3D compressible full Navier-Stokes equation with a Baldwin-Lomax turbulence model [19]. The details of the TF3D solver are not disclosed here, but can be found in [20–22]. Conventional span-wise boundary conditions

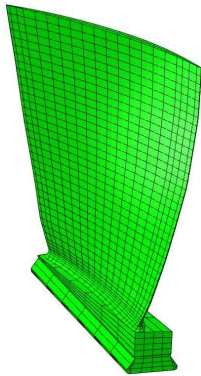


FIGURE 4. EMPLOYED BLADE FINITE ELEMENT MODEL.

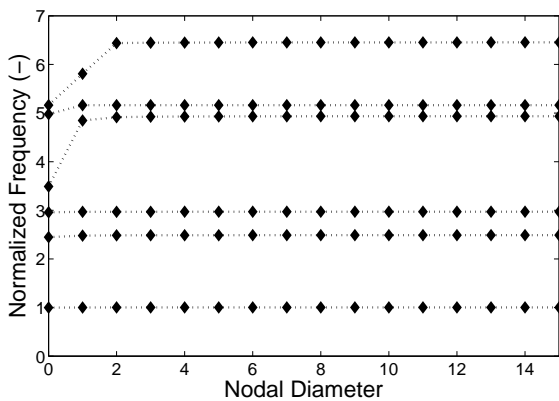


FIGURE 5. NATURAL FREQUENCY VS. NODAL DIAMETER CHARACTERISTICS AT NOMINAL ROTOR SPEED.

are specified at IGV inlet and vane 2 exit. Non-reflective boundaries are enforced. Boundary condition data are acquired from 3D steady state simulations of the whole compressor model, which in turn is calibrated by field-measured performance data. Figure 3(b) illustrates the relative Mach number distribution at midspan for the nominal operating condition ($LP=1.0$). A distinct in-passage shock is clearly visible in rotor 1, which is discussed further below, and one also notes the transonic operation of rotor 2.

Structural Model

The investigated rotor features 31 Titanium blades inserted into a rather sturdy steel disk. Figure 4 depicts the blade part of the used single-sector bladed disk finite element model. Note that the rather coarse finite element mesh is composed of second order brick elements and is therefore fully sufficient for capturing low order modes such as 1F. Figure 5 shows the rotor's eigenfrequency versus nodal diameter characteristics at nominal rotor speed. The eigenmodes of the blade are here calculated by the commercial software ABAQUSTM. Clearly, the visibly stiff

disk in Fig. 1 results in disk eigenfrequencies that are high relative to the blade-dominated ones. In fact, real disk-blade modal interaction does not occur for the three lowest blade mode families, other than a slight softening at low NDs due to marginally increased disk participation in the motion. Consequently, blade-alone 1F modes would conceivably suffice in this case as basis for the aerodynamic damping calculations. However, the investigation later ventures into a mistuning sensitivity assessment and this requires an adequate description of the blade-to-blade structural coupling. Cyclic symmetric assembly modes, or complex traveling wave modes, are therefore used throughout, both for aerodynamic damping calculations and as basis for the mistuned aeromechanical response model.

Mechanical damping for this blade is comprised of material damping (internal hysteresis) and friction damping in the blade-disk attachment. Material damping was measured specifically on this blade design to be about 0.04–0.07% LogDec for the lower modes, employing a weakly suspended (i.e., “free-free”) in-vacuum setup [23]. Given the low material damping and absence of reliable measurements or models of friction damping, both aspects of mechanical damping are fully ignored in this investigation as a precautionary, conservative measure. This is to some degree justified by preliminary evaluations of in-vacuum (i.e., mechanical damping only) spin pit blade vibration measurements, which suggest that 1F mechanical damping is exceptionally low for this rotor.

UNSTEADY BLADE ROW INTERACTION

The interaction between fluid and structure is here assumed to follow the weakly coupled (one-way) approach that may be considered today's standard practice. That is, the airfoil is prescribed to oscillate harmonically in the flow field according to the elastic (in-vacuum) mode shape and at the elastic eigenfrequency. The actual feedback influences on both mode shape and oscillation frequency from fluid inertia and stiffness are thereby ignored. However, this is traditionally considered to be a fair assumption for “normal” turbomachinery blade designs and flow conditions. One of the finite element elastic 1F mode shapes and its interpolation onto the airfoil surface CFD grid are depicted in Fig. 6, showing excellent agreement as expected and required.

The motion-induced unsteady pressures acting on the airfoil are determined using both linear and nonlinear harmonic solvers in TF3D. During unsteady simulations, the computational domain is restricted to rotor 1 only, utilizing a 1D non-reflective boundary formulation at up- and downstream boundaries. The TWM motion of the blades is represented by phase-shifted periodicity over the blade-to-blade boundaries. Note that the tip gap is modeled also in the unsteady analyses.

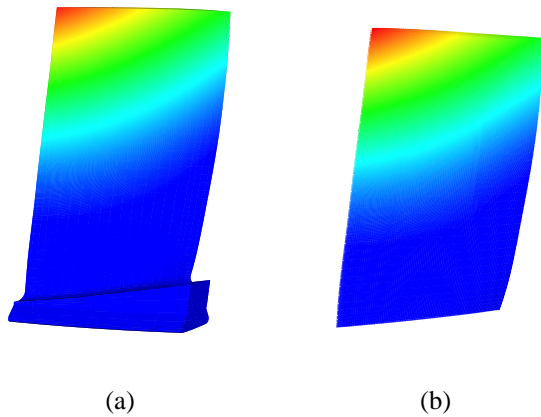


FIGURE 6. TANGENTIAL 1F MODE SHAPE DEFLECTIONS ACCORDING TO THE FINITE ELEMENT MODEL (a) AND AFTER INTERPOLATION ONTO THE CFD GRID (b).

Linear Harmonic Aerodynamic Damping Results

In the linear harmonic simulations, the flow unsteadiness is approximated by the first order flow perturbations varying harmonically with the airfoil oscillation frequency. Furthermore, the maximum blade deflection is specified to 1% of the blade tip chord during the linear harmonic simulations. Figure 7 depicts the obtained 1F aerodynamic damping as function of nodal diameter for the rotor at selected loading parameter values. The large damping range with an envelope of about 16% LogDec signifies an unusually strong aerodynamic coupling for this mode. Moreover, the rather clean first harmonic sinusoidal behavior is evidence that blade-to-blade interaction is limited to the immediate neighbor blades [24].

A zoomed view of the low order forward TWB is also provided in Fig. 7, showing the least stable portion of the “S curve” in more detail. The results presented in Fig. 7 confirm that the nominal operation case is predicted to be stable, as expected and required from service experience. Moreover, the numerical predictions suggest that the nominal case is the most stable operating condition considered here. It is further observed in Figs. 7 and 8 that the least stable condition occurs at LP=0.85. This corresponds to the transition point on the engine power line as indicated in Fig. 8, where obtained minimum aerodynamic damping values are extracted from Fig. 7 and plotted against the loading parameter. At this operating condition, the blade experiences a negative aerodynamic damping as low as -0.5% LogDec for forward traveling 3 ND motion. Thus, under the assumption of a perfectly tuned assembly the rotor is indeed predicted to flutter.

Figures 7 and 8 also reveal that the rotor has a tendency towards instability almost immediately when the loading parameter falls below one. It is further noted that the minimum aerodynamic damping remains essentially at the same level after the

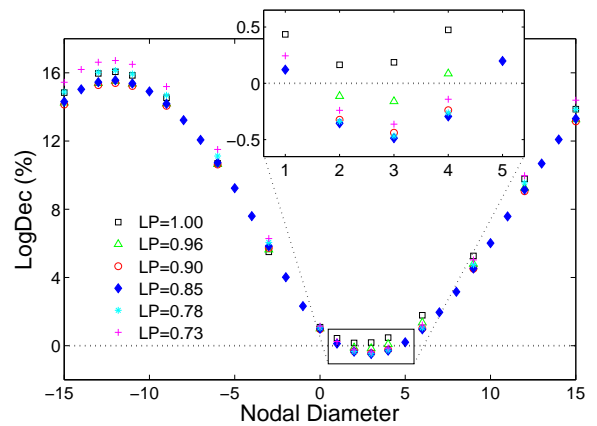


FIGURE 7. MODE 1F AERODYNAMIC DAMPING VS. NODAL DIAMETER FOR DIFFERENT LOADING PARAMETERS, INCLUDING CLOSE-UP VIEW OF MINIMUM DAMPING REGION.

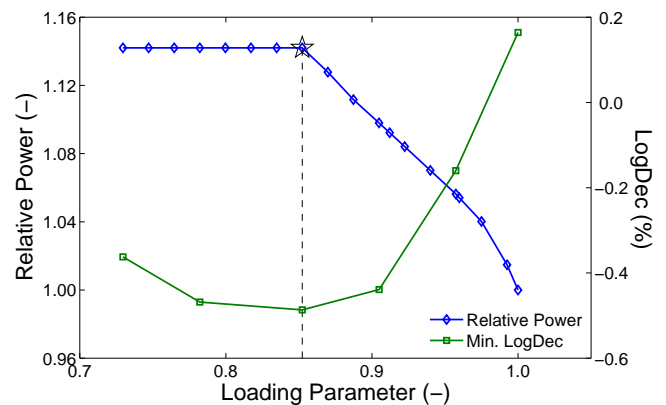


FIGURE 8. EVOLUTION OF ENGINE OUTPUT POWER AND MINIMUM 1F AERODYNAMIC DAMPING WITH LOADING PARAMETER.

transition point. This would indicate that the loading parameter may not be a direct factor influencing aerodynamic damping. Finally, it is observed upon comparing Figs. 2 and 8 that the significant changes in aerodynamic damping over the investigated operating range have no obvious connection with reduced frequency, which varies only marginally. This is also indicated by the monotonic behavior of the reduced frequency contra the non-monotonic behavior of the aerodynamic damping. Hence, the changes in aerodynamic damping must stem from other changes in flow conditions than relative flow speed alone.

To further elaborate on this, Fig. 9 shows the relative Mach number distributions along blade chord at 50% span as obtained from steady state simulations with varying loading parameters. The shock positions on the blade surfaces are easily identified in Fig. 9, and it can be seen that the shock is driven towards the

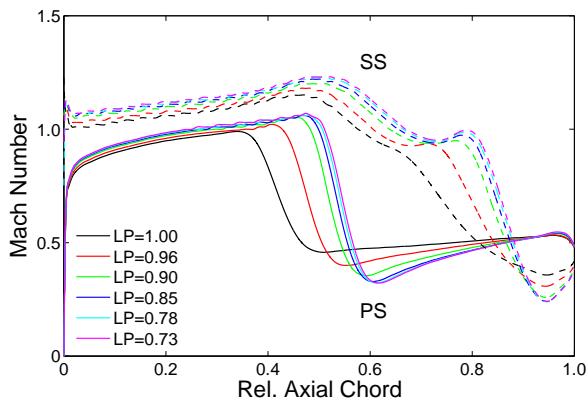


FIGURE 9. STEADY STATE RELATIVE MACH NUMBER DISTRIBUTIONS ALONG BLADE CHORD AT 50% SPAN FOR DIFFERENT LOADING PARAMETERS.

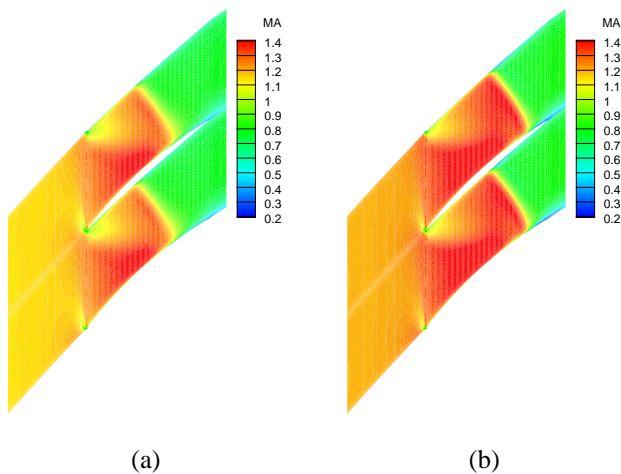


FIGURE 10. STEADY STATE RELATIVE MACH NUMBER DISTRIBUTIONS AT 50% SPAN FOR THE NOMINAL CASE $LP = 1.0$ (a) AND THE LEAST STABLE CASE $LP = 0.85$ (b).

trailing edge as the loading parameter decreases. One can further observe that the shock occupies the region from 80% to 95% of the chord on the suction side in the three lowest loading parameter cases. In other words, the shock attaches near the trailing edge on the blade suction side. This indicates that the rotor operates near fully choked in these three conditions.

Another view is given in Fig. 10, comparing the steady state relative Mach number distribution at midspan between the nominal (stable) and least stable operating cases. The observed high velocity flow in the blade passage generates a strong shock at the trailing edge, and the associated pressure jump becomes larger with increasing flow velocity. In the least stable case, the relative velocity is obviously higher in the front part of the blade

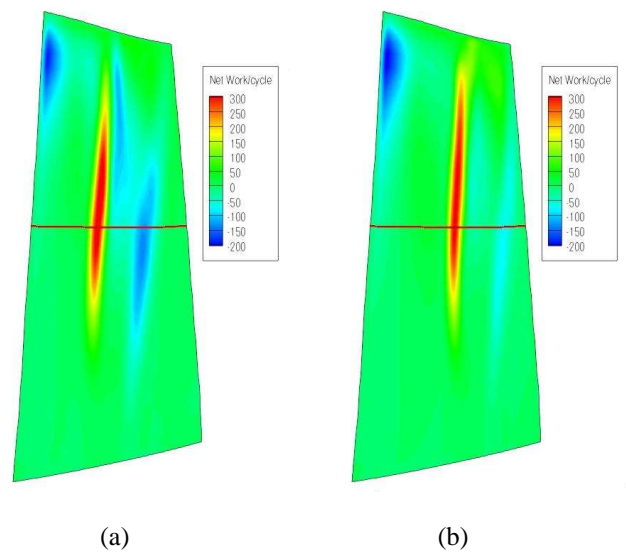


FIGURE 11. MODE 1F NET (PS+SS) AERODYNAMIC WORK DONE ON THE BLADE PER CYCLE FOR THE NOMINAL CASE $LP = 1.0$ (a) AND THE LEAST STABLE CASE $LP = 0.85$ (b).

passage, which leads to a stronger shock and at a position closer to the trailing edge. The stronger shock further indicates a more intensive unsteady force on the blade surfaces.

With no other particular flow features besides the choked condition visible in Figs. 9 and 10, it may be suspected that transonic front stage compressor rotors in general can be subjected to aeroelastic instability risks under similar circumstances. This further highlights the importance of validating aeroelastic instability predictions at such conditions.

Figure 11 provides a comparison between the distributions of aerodynamic work done on the blade per airfoil oscillation cycle in the nominal and least stable cases. The work done is proportional to the imaginary part of the modal force, which is the projection of the airfoil deflections onto the complex unsteady forces acting on the airfoil surfaces. Here, positive values imply that energy is fed into the airfoil (excitation) and negative values signify energy dissipation (damping). It can be observed that the blade part that absorbs the most unsteady aerodynamic work is located around mid-chord from 40% to 80% span in both cases. This stems from shock oscillation on the pressure side. It is further noted that the negative work contribution around midspan, which acts to damp out blade oscillation and stems from shock motion on the suction side, is less prominent in the least stable case than at nominal conditions. On the other hand, the energy dissipation at the leading edge tip region is stronger in the least stable case, but this is a rather localized stabilizing contribution.

Figure 12 gives a more detailed view of the aerodynamic work done on the blade at 50% span (red lines in Fig. 11). Evidently, the maximum local (shock-induced) work contribution

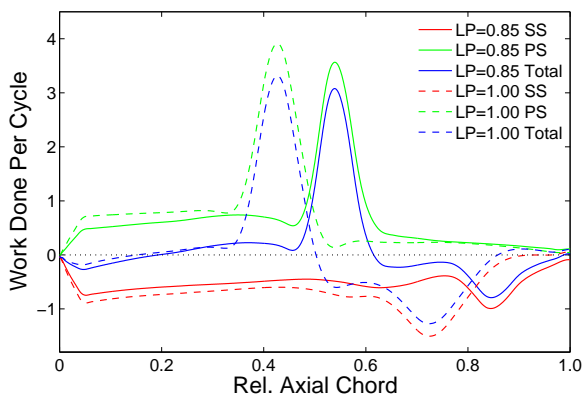


FIGURE 12. AERODYNAMIC WORK DONE PER CYCLE ALONG BLADE CHORD AT 50% SPAN FOR THE NOMINAL CASE $LP = 1.0$ AND THE LEAST STABLE CASE $LP = 0.85$.

on the pressure side is essentially the same in both cases in terms of magnitudes, but its position is driven towards the trailing edge in the least stable case—from 40% of chord to 55%. On the suction side, however, the work that damps the blade (i.e., the integrated area below zero) reduces significantly in the least stable case compared to the nominal case. Hence, changes to the excitation part of the aerodynamic work seem insignificant. Instead, it is the variations in the dissipative aerodynamic work that are believed to be the main reason for the tendency towards aeroelastic instability when going from the nominal case to the least stable case.

Some interim conclusions may be drawn from the linear harmonic results described above. As the loading parameter drops, the shock is driven towards the trailing edge of the airfoil, and the rotor thus driven towards choked condition, until the output power limitation sets in at the transition point. The numerical solutions obtained with the linear harmonic approach show that this transition point constitutes the least stable condition. Moreover, the variation in aerodynamic damping when going from the nominal case to the least stable case stems mainly from changes in dissipative aerodynamic work done on the blade's suction side.

Since the linear harmonic computations lead to the conclusion that the blade can be expected to flutter for low loading parameters, the investigation must logically be expanded to more advanced evaluation techniques. One way ahead is to look at nonlinear flow perturbation effects and the potential for an acceptable limit-cycle oscillation flutter behavior of the blade. This is explored in the next section below.

Nonlinear Harmonic Aerodynamic Damping Results

In the nonlinear harmonic approach also the higher order harmonics of the flow unsteadiness are retained in the solution [20]. This requires a different numerical solver strategy

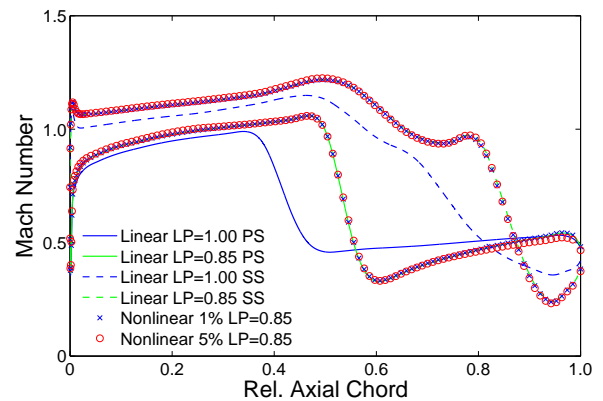


FIGURE 13. COMPARISON OF MEAN RELATIVE MACH NUMBER DISTRIBUTIONS ALONG BLADE CHORD AT 50% SPAN FROM LINEAR AND NONLINEAR SOLUTIONS.

that is more computationally intensive. In this study, the run time required for a nonlinear harmonic simulation was found to be 2–3 times that of the corresponding linear harmonic simulation. Consequently, nonlinear harmonic solutions are currently not considered standard practice. Also, it may be argued that they are unnecessary as long as a design remains stable in the small-amplitude, linear regime. In this investigation, the impact of the higher order harmonics is explored by prescribing airfoil oscillation with amplitudes in the range 0.1–8% of tip chord length by simple mode shape scaling. Hence, also the linear regime is investigated to check the validity of the linear assumption. Finally, note that this study of flow perturbation nonlinearity focuses exclusively on the least stable case ($LP = 0.85$).

In order to address properly how increasing blade oscillation amplitudes affect the nonlinear harmonic response of the system, it seems prudent to first establish if there are any important influences on the mean flow about which the solution varies periodically. In terms of overall behavior, the rotor's mean pressure ratio and polytropic efficiency are found to remain within 0.0002 and 0.1%, respectively. A more detailed view is illustrated in Fig. 13, showing the relative Mach number distribution along the chord at 50% span for the least stable case ($LP = 0.85$). The steady state data for the nominal case ($LP = 1.0$) is also included in order to put the linear (i.e., steady state) versus nonlinear mean differences in perspective. It is observed that the nonlinear harmonic averages follow the steady state solution very closely, also in the 5% amplitude case. As a measure of the nonlinear influence, it is noted that the maximum deviation in mean relative Mach number at any given point along the chord is only 2% in the 1% amplitude case. The corresponding number for the 5% amplitude case is 5% deviation. These maximum deviations occur in both cases quite locally around the suction side shock attachment near the trailing edge. This is not entirely unexpected, since this location exhibits a combination of large mode deflection and a significant

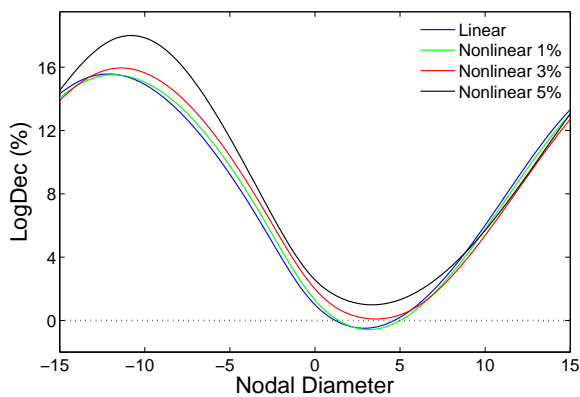


FIGURE 14. MODE 1F AERODYNAMIC DAMPING VS. NODAL DIAMETER FROM LINEAR AND NONLINEAR HARMONIC SOLUTIONS.

jump in pressure across the shock wave. In view of the above, it is concluded that deviations to the mean flow induced by nonlinearity will likely have a rather marginal influence on observed changes to the aerodynamic damping as oscillation amplitudes increase beyond the linear regime. However, the slightly reduced mean flow velocity in the suction side trailing edge region could potentially contribute to the observed changes in unsteady pressure phase in this location that are reported below.

The predicted aerodynamic damping from both linear and nonlinear harmonic simulations are compared in Fig. 14. It can be deduced from Fig. 14 that nothing dramatic happens to the aerodynamically coupled system as oscillation amplitudes increase. The coupling between neighboring blades (i.e., “S curve” amplitude) remains about the same, while the dissipative work performed by the blade on itself (i.e., “S curve” average) increases gradually as oscillation amplitudes increase beyond the linear regime. Based on extracted minima from obtained “S curves” Fig. 15 illustrates how the minimum 1F aerodynamic damping varies with increasing mode oscillation amplitude up to 8% of tip chord length. The first observation made is that the minimum aerodynamic damping from linear and nonlinear harmonic simulations agree well for sufficiently small deflection amplitudes. In this case, the limit appears to be at about 1.5–2% of chord length. Thus, the obtained results seem to confirm the appropriateness of the linear harmonic assumption for small vibrations.

As blade amplitudes grow larger, the nonlinear solutions start to deviate significantly relative to the linear result. In fact, the nonlinear simulations seem to indicate an “almost linear” relationship between minimum aerodynamic damping and oscillation amplitude when the deflection is in the range of approximately 1.5 to 6% of chord length. Note that this type of relationship is in accordance with previous work [11]. Based on the results displayed in Fig. 15 and under the assumption of a

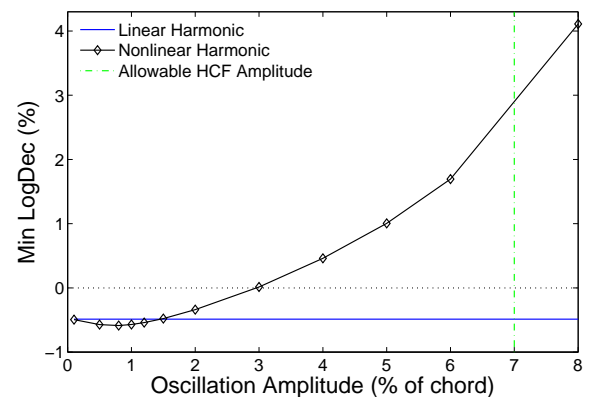


FIGURE 15. MINIMUM 1F AERODYNAMIC DAMPING AS FUNCTION OF BLADE OSCILLATION AMPLITUDE.

fully tuned assembly, one can deduce that the numerical simulations predict that the blade will start to flutter from white noise-type vibrations with increasing vibration amplitude for each accumulated oscillation cycle. As the blade reaches vibration amplitudes of approximately 3% of tip chord length the blade becomes neutrally stable, i.e., slightly higher amplitudes will be damped downward and slightly lower amplitudes will be excited upward. Thus, a state of limit-cycle oscillation would be reached. To this end, it should be noted that the HCF design limit for this blade’s 1F mode corresponds to an amplitude of about 7% of chord length. A limit-cycle oscillation amplitude of 3% of chord length would thus be acceptable (in theory).

Figure 16 illustrates the unsteady pressure amplitude and phase distributions on the airfoil surface according to the linear harmonic solution and the nonlinear harmonic solutions with 1% and 5% of chord length oscillation amplitudes. The unsteady pressure amplitudes at 5% amplitude are linearly scaled back to facilitate the back-to-back comparison in Fig. 16. Note that the amplitude is irrelevant in the linear harmonic case.

As mentioned before, the in-passage shock attaches to the blade surface and the highest unsteady pressure amplitudes on the airfoil surface stem from shock oscillation. Comparing the linear and nonlinear solutions with 1% amplitude, the shown smoothing of the unsteady pressure for the nonlinear solution is rather expected. Figure 16 further shows that the pressure phase is nearly identical between these two cases. Apparently, there is a further smoothing (in relative terms) of the shock-induced unsteady pressure as the oscillation amplitude increases to 5%, but only on the lower half of the blade. Looking towards the blade tip, one finds instead that the shock-induced pressure amplitudes increase in relative terms for the higher oscillation amplitude. This is found to be the case for both suction and pressure sides. Meanwhile, the phase distribution of the shock-induced unsteady pressures varies moderately but noticeably as the vibration amplitude increases from 1% to 5%. Two

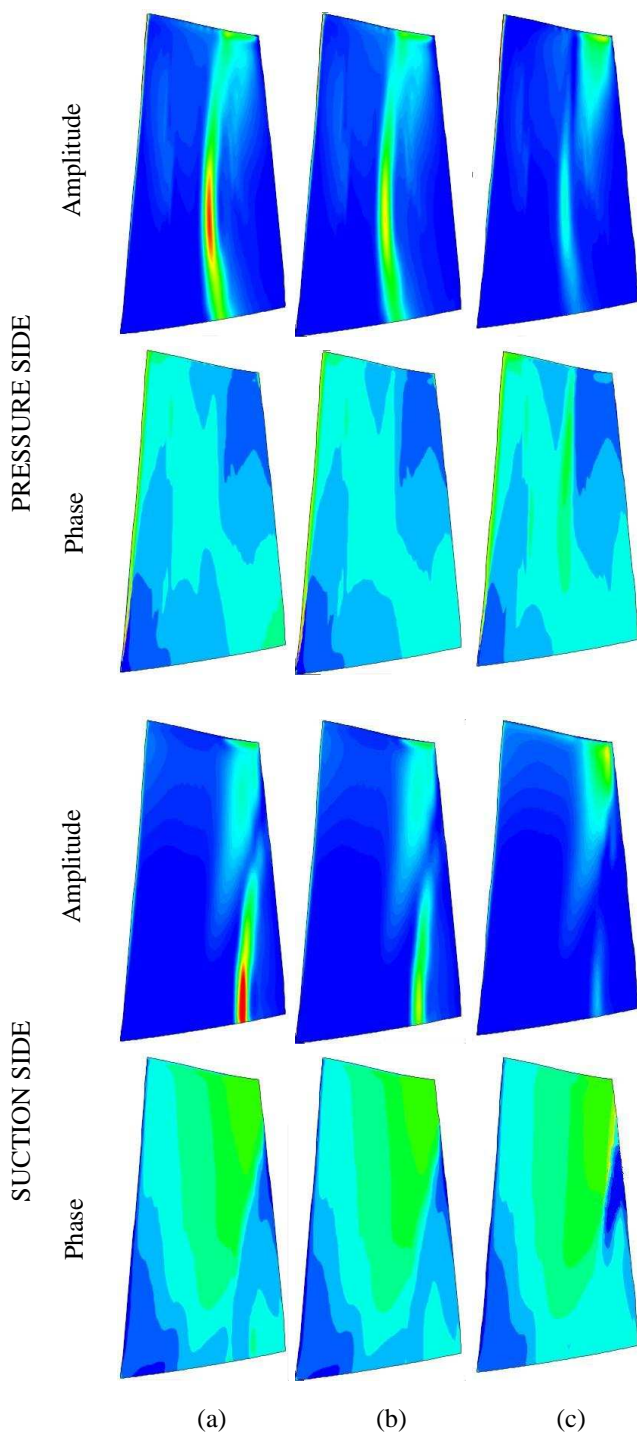


FIGURE 16. UNSTEADY PRESSURE AMPLITUDE AND PHASE DISTRIBUTIONS DUE TO 1F MOTION PER % CHORD AMPLITUDE: (a) LINEAR HARMONIC SOLUTION WITH 1% OF CHORD AMPLITUDE; (b) NONLINEAR HARMONIC SOLUTION WITH 1% OF CHORD AMPLITUDE; (c) NONLINEAR HARMONIC SOLUTION WITH 5% OF CHORD AMPLITUDE.

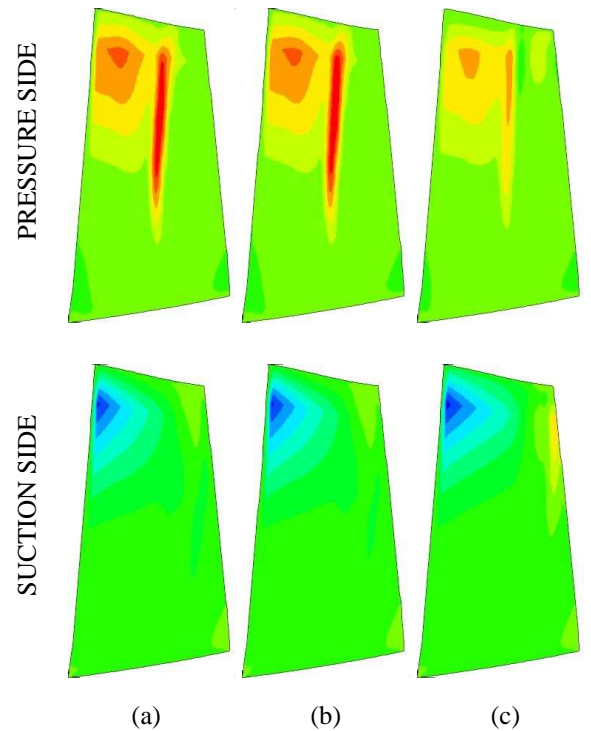


FIGURE 17. AERODYNAMIC WORK DONE PER CYCLE DISTRIBUTIONS DUE TO 1F MOTION PER % CHORD AMPLITUDE: (a) LINEAR HARMONIC SOLUTION WITH 1% OF CHORD AMPLITUDE; (b) NONLINEAR HARMONIC SOLUTION WITH 1% OF CHORD AMPLITUDE; (c) NONLINEAR HARMONIC SOLUTION WITH 5% OF CHORD AMPLITUDE.

of the most prominent changes in this regard are that the shock-induced unsteady pressures are phase-shifted ahead slightly in the midspan region on the pressure side and around 80% span on the suction side. Obviously, the changes to the shock-induced pressure amplitudes and their phase due to flow perturbation non-linearity will both influence the aerodynamic work done on the blade. However, the understanding of the underlying mechanisms that are responsible for this nonlinear flow perturbation behavior is deferred to future, more in-depth investigations.

Figure 17 provides a comparison of the aerodynamic work done on the blade for the same cases as in Fig. 16. Again, the 5% amplitude case displayed in Fig. 17(c) is linearly scaled back to facilitate the comparison, but now by the relative amplitude change squared. As one would expect based on the Fig. 16 data, the work distribution on both pressure and suction sides are essentially identical between linear and nonlinear solutions within the linear regime (1% amplitude). The changes in shock-induced pressure amplitudes discussed above have limited impact in this regard. The reason for this being that the significant pressure amplitude changes occur on the blade's lower half, whereas the pri-

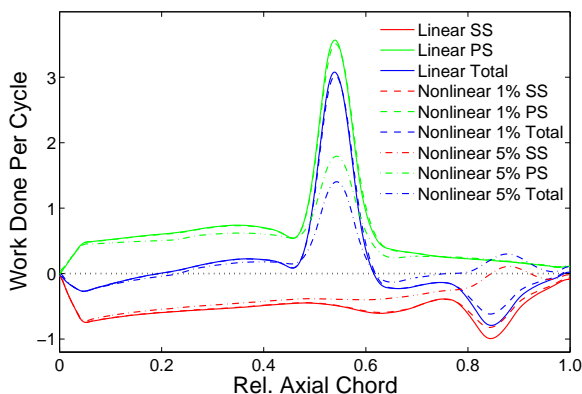


FIGURE 18. AERODYNAMIC WORK DONE PER CYCLE ALONG BLADE CHORD AT 50% SPAN FROM LINEAR AND NONLINEAR HARMONIC SOLUTIONS.

many positive and negative work contributions are located around midspan and above. This is not entirely surprising as blade deflection increases with span.

For the 5% amplitude case, the shock-induced pressure amplitudes on the pressure side reduce also on the upper half of the blade, which then has a direct impact on the work done on the blade as seen in Fig. 17(c). Meanwhile, on the suction side, a new destabilizing zone is forming on the upper half near the trailing edge, which corresponds to a zone of phase-shifted, high-intensity unsteady forces that appears in the nonlinear, high-amplitude solution. A local but more detailed view of these changes is provided in Fig. 18, showing the aerodynamic work done per oscillation cycle distribution along the chord at 50% span. It is observed from Fig. 18 that the excitation peak on the pressure side reduces to about half of that at 1% amplitude, while the suction side dissipation peak towards the trailing edge vanishes completely and even turns into a zone of excitation. In other words, the nonlinearity at high amplitudes results in competing effects on either side of the airfoil. However, the excitation decrease on the pressure side outweighs the loss of dissipation on the suction side such that the net effect has turned the blade aeroelastically stable.

It can be concluded here that the linear harmonic approach agrees well with the nonlinear harmonic approach as long as vibratory amplitudes stay relatively small. It is found that for this specific case the blade turns stable as the amplitude grows larger, leading to a state of limit-cycle oscillations. According to the performed computations, the key to this aeroelastic stabilization is a substantial reduction (in relative terms) in shock-induced unsteady pressure amplitudes on the upper half of the blade's pressure side.

MISTUNING EFFECTS

All prior analyses in the presented investigation have assumed that the bladed disk assembly is tuned, i.e., a perfectly cyclic symmetric assembly with identical blades. In reality, this can never be achieved (if at all desirable) due to manufacturing tolerances, material flaws, in-service wear, etc., which is commonly denoted mistuning. This ever-present asymmetry, or mistuning, in a bladed disk influences both the aerodynamic flow field and its structural dynamics behavior, with the influence on the latter being distinctly non-proportional in many cases. In particular, it may lead to drastically increased forced response amplitudes of the system, but it has also the potential to mitigate flutter by mode localization. For obvious reasons, the flutter mitigation aspect is the primary interest in this investigation.

Mistuned Aeromechanical Response Model

The mistuned aeromechanical analyses are carried out using an in-house implementation of the mistuning projection method presented by Bladh *et al.* [25]. The original method is here adapted to complex-valued TWMs and expanded to include aerodynamic coupling. In this approach, the structural deviations (mass and/or stiffness) of the individual blades or bladed disk sectors are projected along the tuned modal basis. The employed reduced order model further implies the conventional assumption of a linear system undergoing harmonic motion. Consequently, the mode-wise aerodynamic coupling terms are assumed to be linear functions of modal amplitude and are implemented as complex-valued stiffness contributions.

One key attractiveness of this approach is that it allows for complex modal interaction between blade mode families, as well as between blade and disk modes, while keeping the response model size and hence computational effort at a minimum. Secondly, it uses modal data that is normally readily available as part of the design process, i.e., the cyclic symmetry modes of a bladed disk sector. Thirdly, its modal basis is identical to that typically used in aeroelastic analyses yielding the aerodynamic coupling coefficients. The key limitation is the restriction to unperturbed airfoil mode shapes and hence to what is referred to as small mistuning due to tolerances etc.

To set up the response model one needs only the cyclic symmetric TWMs and the stiffness and/or mass matrices for the structural part that is to be considered mistuned. In this case, the blade alone depicted in Fig. 4 is assumed to be mistuned. The mistuned assessment presented here considers only the simplest form of mistuning, i.e., a uniform perturbation of the stiffness matrix, which is equivalent to a variation in Young's modulus. Since the 1F mode family is well isolated from other modes as shown in Fig. 5, it suffices to use the set of 1F TWMs only as modal basis. Hence, the size of the response model is only 31 DOF. The 1F cyclic symmetry modes and the blade-alone stiffness matrix are calculated by ABAQUSTM. For consistency,

these modes are exactly the same as those used for the harmonic aerodynamic damping analyses reported above.

Furthermore, this investigation encompasses a feasibility study related to the use of statically condensed matrices by means of Guyan reduction [26] as basis for the mistuning projection. The incentive is to be able to reduce the storage size of the data involved when constructing the response model. For instance, the number of finite element DOF in a refined model of a cooled turbine blade can easily reach into the millions, and the extracted structural matrices then become prohibitively, or at least impractically, large in terms of data storage and handling.

Guyan reduction implies that a structure is divided into physically retained master (active) DOF and slave (passive) DOF. Based on the statics problem, the slave DOF can be expressed in terms of master DOF and are thus eliminated from the system, while associated slave stiffness and mass contributions get lumped onto the retained master DOF. In statics, this model condensation is exact and is commonly referred to as substructuring. In a structural dynamics context, Guyan reduction is an approximation and is the equivalent of using only the static constraint modes as modal basis, i.e., shapes induced by unit deflections of each retained master DOF. Consequently, its suitability for dynamic condensation is typically somewhat limited, as the imposed constraints on structural motion may lead to a substantial increase in dynamic stiffness depending on the choice of master DOF [14]. Nevertheless, this master DOF selection sensitivity is expected to be less pronounced when this reduction method is used as basis for perturbations only.

For this investigation a series of progressively coarser master DOF configurations are defined in a systematic manner. The corresponding condensed stiffness matrices are extracted directly within ABAQUSTM. In truth, the present blade-alone finite element model depicted in Fig. 4 does not require the proposed static condensation as the number of DOF is only around 30,000. However, it serves well the purpose of demonstration.

Figure 19 illustrates the accuracy of the condensed matrices relative to the full finite element matrix representation. The accuracy is measured in terms of mistuned eigenfrequency errors and the classical modal assurance criterion, MAC [27], which is here expanded to complex-valued mode shapes:

$$MAC = \frac{(\mathbf{u}_1^* \cdot \mathbf{u}_2)^* \cdot (\mathbf{u}_1^* \cdot \mathbf{u}_2)}{(\mathbf{u}_1^* \cdot \mathbf{u}_1)^* \cdot (\mathbf{u}_2^* \cdot \mathbf{u}_2)} \quad (2)$$

The mode shape vectors \mathbf{u}_1 and \mathbf{u}_2 are comprised of the relative strain energy of the 31 blades for response models using Guyan-reduced matrices and the full matrix, respectively. The mistuned mode shape and eigenfrequency comparisons in Fig. 19 are based on all 31 mistuned modes obtained for a representative mistuned configuration from impact testing. The solid lines represent the MAC and eigenfrequency error averages among the

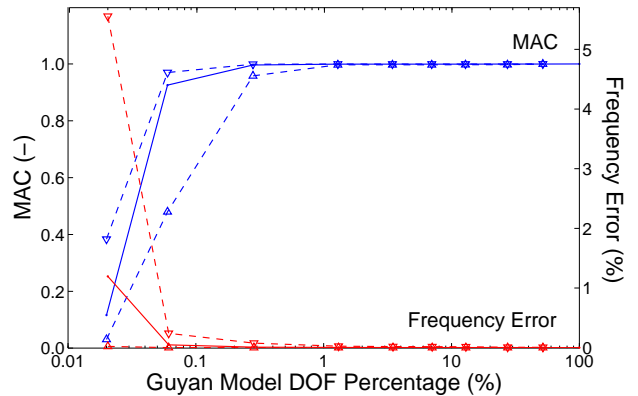


FIGURE 19. EVOLUTION OF AVERAGE (solid) AND MIN/MAX (dashed) MISTUNED MAC VALUES AND EIGENFREQUENCY ERRORS VS. THE NUMBER OF RETAINED MASTER DOF.

31 modes for each Guyan reduction model, while the dashed lines are generated from the corresponding maximum and minimum values. Clearly, using a Guyan-reduced stiffness matrix yields (for this model) acceptable response model performance for quite low fractions of retained master DOF. Looking at the eigenfrequency errors alone the retained DOF fraction could be taken as far down as 0.1%, since eigenfrequency errors within 0.2% are deemed acceptable for all practical purposes. However, the accurate capture of mistuned mode shape characteristics (e.g., localization) is critical for the ensuing analyses and thus determines the model reduction limit to about 1%. Below this level the mistuned mode shape representation starts to deteriorate, with certain modes being unacceptably far off target for reliable mistuned aeromechanical response calculations. Finally, note that the Guyan reduction model employed in the remainder of this section contains 4% retained master DOF.

Mistuned Aeroelastic Stability Assessment

As mentioned in the introduction it is well known that mistuning improves aeroelastic stability, which is dictated by the minimum aerodynamic damping. The mechanism behind this is that mistuning leads to more or less localized modes, implying that several and quite possibly all the tuned TWMs participate in the motion. As a consequence, the effective aerodynamic damping of the mistuned, localized mode is a composite damping comprised of the aerodynamic damping of all the tuned TWMs weighted by the TWMs' respective participation in the motion. Thus, mistuned aerodynamic damping will always be higher than the minimum and, conversely, lower than the maximum tuned aerodynamic damping.

Intentional mistuning in general and alternating mistuning in particular have been shown to be especially effective in this regard, and the technique has also been used successfully in prac-

tice to mitigate flutter tendencies. Alternating mistuning requires two blade types with a defined eigenfrequency offset, where the two blade types are placed alternately around the wheel. This type of arrangement is reasonable also from a practical-economic standpoint as long as the required frequency offset is within reason. Note that some form of intentional mistuning is in a sense always introduced in practice, since the blades are placed with respect to mass and second moments for rotor balancing purposes. However, a true intentional mistuning pattern with a defined frequency offset is of course preferable in terms of controllability and robustness.

The mistuned stability assessment is done for the least stable condition from the linear harmonic computations above ($LP = 0.85$). The study focuses on experience-based random mistuning levels from today's manufacturing standards, implying 1F eigenfrequency standard deviations in the range 0.5–0.85%. Intentional mistuning is considered in the form of alternating mistuning such that every second blade in the nominal (tuned) configuration is replaced by a higher-frequency blade. Note that with an odd number of blades (31) only a “near-alternate” configuration can be achieved. Moreover, as manufacturing tolerances etc. have to be treated as random quantities, a probabilistic assessment is done with and without intentional mistuning through Monte Carlo simulations using 10,000 random configurations at each random mistuning level. Random mistuning parameters are here taken from a Gaussian distribution, which gives an adequate representation of measured frequency deviations.

The results from the Monte Carlo simulations are shown in Fig. 20, where the flutter probability at each level of mistuning standard deviation is simply the fraction of mistuned configurations exhibiting unstable modes out of the total 10,000. Figure 20 shows how the flutter risk (probability) is drastically reduced even for a rather modest intentional mistuning with 0.5% frequency offset. Furthermore, the flutter risk is found to decrease rapidly with increasing random mistuning in the range expected from manufacturing. Hence, from the perspective of this investigation, a tightening of tolerances is not desirable. It is further noted that the results with and without Guyan reduction are reasonably close, and also that the Guyan reduction model seems to yield conservative results in this regard. The latter observation is rather counter-intuitive in the authors' opinion. As mentioned earlier, constraining a structure to deform in accordance with a truncated set of static deflection shapes increases its dynamic stiffness. Considering that mistuning perturbations are here implemented as fractions of the Guyan-reduced stiffness matrix, one would therefore expect the perturbations to be overestimated. This would in turn lead to a more rapid stabilization compared to using the full finite element matrices. However, the exact opposite is observed here.

For a balanced judgment of the flutter risk it is realized that the standard deviation of random (manufacturing) mistuning is also a random variable with some distribution that may or may

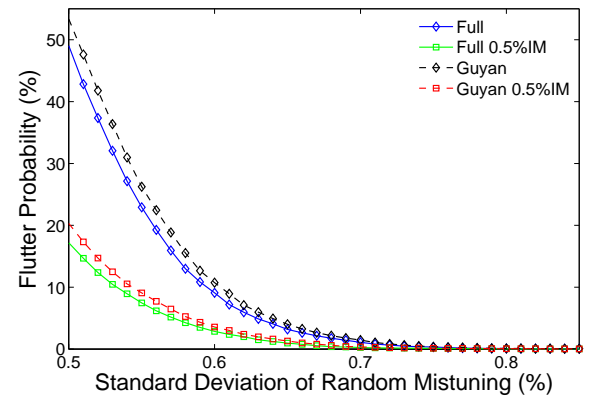


FIGURE 20. FLUTTER PROBABILITY VARIATION WITH STANDARD DEVIATION OF RANDOM FREQUENCY MISTUNING FOR DIFFERENT LEVELS OF INTENTIONAL MISTUNING.

not be known. In this case it is not known and it is therefore assumed that the standard deviation of random mistuning is a uniformly distributed variable, i.e., it is with equal probability anywhere in the defined range 0.5–0.85%. Each vertical slice in Fig. 20 has then equal weight, implying that the total flutter probability is simply the average within the anticipated standard deviation range. With this simplification, the estimated total flutter risk using the full matrix model becomes 8.8% without intentional mistuning and 2.9% with an alternating blade frequency offset of 0.5%. The corresponding numbers using the Guyan reduction model are somewhat higher: 10.1% and 3.5%, respectively. Hence, the flutter risk drops quickly as alternating mistuning is introduced and becomes negligible for frequency offsets of 1% and beyond.

Figure 21 depicts the root loci of tuned and mistuned eigenmodes using the same measured randomly mistuned configuration as in the Guyan DOF convergence study (Fig. 19), having a standard deviation of 0.5%. Three cases are displayed: (i) tuned case; (ii) randomly mistuned configuration (RM); and (iii) 1.2% alternating intentional mistuning plus randomly mistuned configuration (1.2%IM+RM). Note that there is only one tuned model, since Guyan-reduced matrices are used for perturbations only. It is seen that the randomly mistuned configuration has a rather limited stabilizing effect on the system. Alternating intentional mistuning on the other hand stabilizes the system very effectively at the expense of a wider frequency spread. It is notable that although the intentionally mistuned blades have a defined offset, the root loci are not separated into two groups in terms of frequency. This is explained by the circumstance that the randomly mistuned configuration features frequency deviations of the same order as the defined alternating frequency offset. Interestingly, the Guyan reduction model here behaves according to expectation, i.e., the Guyan reduction model gives a higher degree of stabilization for a given mistuned configuration (the RM case in

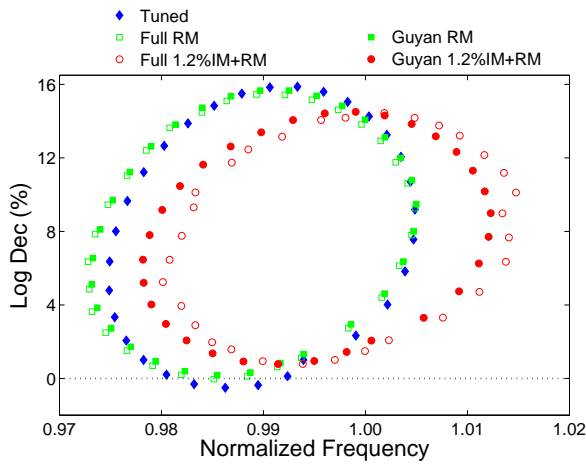


FIGURE 21. TUNED AND MISTUNED EIGENMODE ROOT LOCI DISTRIBUTIONS FOR SELECTED MISTUNED CONFIGURATIONS.

particular). It is further noted that the Guyan reduction model seems to perform progressively worse as the mistuning level increases.

It can be concluded from this mistuned aeroelastic stability assessment that flutter mitigation is effectively achieved for this rotor by means of alternating mistuning with practically feasible frequency offset levels. In fact, the required offset level is of the same order as expected random mistuning levels from manufacturing. In other words, it may be possible to achieve a near-enough alternating pattern with existing production blades, alleviating the need for a second blade design. It is further noted from performed statistical analyses that the Guyan reduction model yields slightly higher and thus conservative flutter probabilities compared to the full model. An in-depth investigation into this seemingly counter-intuitive behavior is beyond the scope of this study and is deferred to future research. Consequently, it is also impossible to judge here the generality of the apparent conservative nature of the Guyan reduction model in connection with mistuned aeroelastic stability assessments.

Mistuned Response Assessment

Although it is found in the previous section that alternating intentional mistuning has a positive effect on flutter mitigation, it may have a detrimental effect on forced response amplitudes. Hence, a final study is performed here to establish its impact on the system's forced response behavior.

There are several publications discussing the merits of intentional mistuning also in the forced response, e.g., [28, 29]. It is found that intentional mistuning typically cuts the forced response amplification peak that is often seen for randomly mistuned systems with low damping. However, it has also been

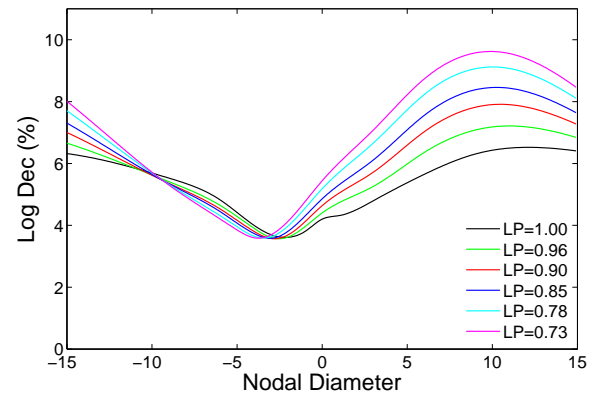


FIGURE 22. MODE 3 AERODYNAMIC DAMPING VS. NODAL DIAMETER FOR DIFFERENT LOADING PARAMETERS.

found that the intentionally mistuned system remains at a stable amplification level as mistuning increases. Meanwhile, the amplification for a randomly mistuned system can drop significantly after the peak is passed and fall below that of the intentionally mistuned system. Hence, the impact of intentional mistuning on forced response amplitudes may be positive or negative depending on interblade coupling, damping, and mistuning levels.

The forced response check is done for a backward traveling 7 EO excitation interfering with mode 3. Since this response assessment is of relative nature, a single 3D dummy force of unit magnitude is applied at blade tip, leading edge. The same type of aeromechanical response model as in the previous section is employed, but now constructed from mode 3 TWMs and associated aerodynamic coupling coefficients. Although the operating point could be chosen arbitrarily for this forced response check, structural model data and aerodynamic coupling coefficients for loading parameter 0.85 are utilized also in this case. The mode 3 linear harmonic aerodynamic damping curves for several operating points are shown in Fig. 22. Unlike the 1F mode, mode 3 is solidly stable and exhibits a significantly weaker blade-to-blade aerodynamic coupling. Finally, an assumed total mechanical damping of 0.2% LogDec is introduced in order to facilitate a comparison of response amplification characteristics considering only structural coupling on one hand, and both structural and aerodynamic coupling on the other.

Figure 23 provides the envelopes of maximum relative response amplitudes (i.e., relative to the tuned peak response) for nearly the same configurations as in Fig. 21: (i) tuned case; (ii) randomly mistuned configuration (RM); (iii) 1.2% alternating intentional mistuning (1.2%IM); and (iv) 1.2% alternating intentional mistuning plus randomly mistuned configuration (1.2%IM+RM). The figure reveals the expected spread in resonant frequencies as the system is mistuned. Magnification levels are seen to be rather modest in this case (less than 25%), depending in part on low mistuning sensitivity but also on modifications

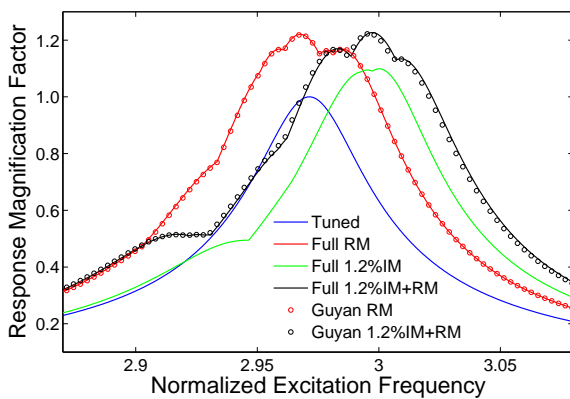


FIGURE 23. ENVELOPE OF MAXIMUM RELATIVE FORCED RESPONSE AMPLITUDES FOR SELECTED MISTUNED CONFIGURATIONS.

to the aerodynamic damping due to mode localization. Figure 23 also shows evidence of the fact that the randomly mistuned frequency deviations are of the same order as the intentional frequency offset, which was alluded to in the previous section. Interestingly, the Guyan reduction model does not show at all the same signs of deterioration for case (iv) in the forced response as it did in the 1F stability analysis (Fig. 21). Although interesting, it is impossible from Fig. 23 to draw any conclusions on the impact on the forced response from introducing alternating mistuning, since the results refer to one specific randomly mistuned configuration only. For this, one needs instead to look at the forced response statistics.

Figure 24 provides a comparison of the 99.9th percentile response magnification factors for different levels of intentional mistuning of the structurally coupled system versus the system featuring both aerodynamic and structural coupling. Again, response amplitudes are normalized with respect to the corresponding system's tuned peak response amplitude. The results show that a magnification reduction can be expected in both systems from intentional mistuning for relevant mistuning levels, but also that the reduction in both cases is rather modest. From a structural point of view, promoting certain ND motion by intentional mistuning will reduce somewhat the structure's possibility to confine energy. This would be responsible for the observed reduction in magnification factor for the structurally coupled system. When aerodynamic coupling is added the situation becomes more complex, since the promotion of certain ND motion will also promote the aerodynamic damping levels of these NDs. This can obviously have a significant effect on the response amplification for the aerodynamically coupled system, as it could either increase response levels (lower damping) or decrease them (higher damping). A second aspect of aerodynamic coupling is the aerodynamic stiffness and inertia, which will introduce an ND-dependent offset to the system's elastic eigenfrequencies.

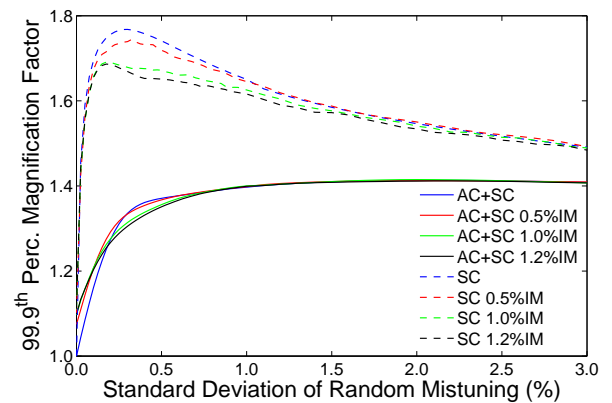


FIGURE 24. 99.9th PERCENTILE RESPONSE MAGNIFICATION FACTORS VS. STANDARD DEVIATION OF RANDOM FREQUENCY MISTUNING WITH AND WITHOUT AERODYNAMIC COUPLING AND FOR VARYING LEVELS OF INTENTIONAL MISTUNING.

Hence, the modal density is reduced compared to that of the structurally coupled system, which typically makes the system less prone to energy confinement for a given level of intentional mistuning. With this last aspect in mind, the results shown in Fig. 24 make sense. That is, the benefit of intentional mistuning seen in the structurally coupled system is also observed after the addition of aerodynamic coupling, but to a much lesser degree. This is also consistent with the observation that the peak magnification is reduced and shifted towards higher mistuning levels as interblade coupling increases.

Finally, it is concluded from the performed computations of mistuned response statistics that resonance amplitudes can with 99.9% certainty be expected to amplify by at most 40% for the aerodynamically coupled system of practical interest here. In the authors' experience, this level of response magnification is by no means unique for the lower modes of this type of blade that feature a combination of rather weak structural coupling and significant levels of aerodynamic coupling. Furthermore, Fig. 24 shows that alternating intentional mistuning does not have a decisive impact on the forced response amplitude at the studied resonance. Nevertheless, the obtained results do indicate that there is some marginal benefit from alternating mistuning in the frequency standard deviation range 0.3–0.8%, which is a highly relevant range for the blade design in question.

SUMMARY & CONCLUSIONS

A comprehensive investigation into the aeroelastic stability behavior of a transonic front blade in an industrial compressor has been performed, utilizing state-of-the-art tools and methods available to the turbomachinery industries today. The evolution of airfoil stability in the first flexural mode is studied as

the front blade operation progresses towards fully choked condition. A weakly coupled (one-way) approach is employed to describe the interaction between fluid and structure. Steady state aerodynamics and the motion-induced unsteady pressures acting on the airfoil are determined using an in-house 3D Navier-Stokes flow solver. Both linear and nonlinear harmonic formulations are used to simulate the unsteady aerodynamics.

The destabilizing mechanism is found to be distinctly shock-driven. Consequently, the aerodynamic work done on the blade changes as the in-passage shock migrates downstream and intensifies when operating conditions progress towards choke condition. As the blade is found prone to flutter in the small-amplitude, linear regime, the study moves on to explore the impacts of flow perturbation nonlinearity as well as structural mistuning.

Aerodynamic damping is found to increase essentially linearly with blade oscillation amplitude as amplitudes grow beyond the linear regime. In fact, the performed nonlinear harmonic simulations show that the rotor becomes aeroelastically stable well before reaching integrity-endangering amplitudes with respect to high cycle fatigue limits. Hence, a safe limit-cycle oscillation situation is predicted for the fully tuned blade.

Additionally, reverting back to the unstable linear harmonic results, a thorough statistical investigation of the stabilizing impact of random and intentional mistuning has been performed based on today's blade manufacturing precision. As expected, it is found that the stabilizing effect of alternating mistuning is vastly superior, in addition to being more easily controllable and therefore robust. It is further shown that intentional mistuning using a quite feasible 1% blade frequency offset can be expected to alleviate the predicted flutter risk. As a final check, it is confirmed that utilization of alternating mistuning has a beneficial effect also in the forced response relative to the inevitable random blade mistuning. In conclusion, alternating intentional mistuning at a practically feasible level has here been shown to be a viable solution towards eliminating a potential flutter problem for the industrial compressor rotor in question.

ACKNOWLEDGMENT

The authors wish to thank Siemens Industrial Turbomachinery AB, Finspong, Sweden, for the permission to publish this material. Additionally, the authors gratefully acknowledge all individuals who have supported the process of writing this paper.

REFERENCES

[1] Carter, T. J., 2005. "Common Failures in Gas Turbine Blades". *Engineering Failure Analysis*, **12**(2), pp. 237–247.

[2] Simmons, H. R., Brun, K., and Cheruvu, S., 2006. "Aerodynamic Instability Effects on Compressor Blade Fail-

ure: A Root Cause Failure Analysis". ASME Paper No. GT2006-42401.

- [3] Chan, K. S., Enright, M. P., Simmons, H. R., Golden, P. J., Chandra, R., and Pentz, A. C., 2010. "Toward Developing a Probabilistic Methodology for Predicting High-Cycle Fretting Fatigue in Aero-Engines". ASME Paper No. GT2010-23007.
- [4] Mazur, Z., Hernández-Rossette, A., and Porcayo-Calderón, J. A., 2010. "Failure Investigation of the 69 MW Gas Turbine of a Combined Cycle Unit". ASME Paper No. GT2010-22262.
- [5] Giles, M. B., 1990. "Stator/Rotor Interaction in a Transonic Turbine". *Journal of Propulsion and Power*, **6**(5), pp. 621–627.
- [6] Moffatt, S., and He, L., 2005. "On Decoupled and Fully-Coupled Methods for Blade Forced Response Prediction". *Journal of Fluids and Structures*, **20**(2), pp. 217–234.
- [7] Vahdati, M., Simpson, G., and Imregun, M., 2008. "Unsteady Flow and Aeroelasticity Behavior of Aeroengine Core Compressors During Rotating Stall and Surge". *Journal of Turbomachinery*, **130**(3), pp. 031017.
- [8] Sanders, A. J., 2005. "Nonsynchronous Vibration (NSV) due to a Flow-Induced Aerodynamic Instability in a Composite Fan Stator". *Journal of Turbomachinery*, **127**(2), pp. 412–421.
- [9] Huang, X. Q., He, L., and Bell, D. L., 2009. "Experimental and Computational Study of Oscillating Turbine Cascade and Influence of Part-Span Shrouds". *Journal of Fluids Engineering*, **131**(5), pp. 051102.
- [10] Sanders, A. J., Hassan, K. K., and Rabe, D. C., 2004. "Experimental and Numerical Study of Stall Flutter in a Transonic Low-Aspect Ratio Fan Blisk". *Journal of Turbomachinery*, **126**(1), pp. 166–174.
- [11] Lee, C. L., 1986. "An Iterative Procedure for Nonlinear Flutter Analysis". *AIAA Journal*, **24**(5), pp. 833–840.
- [12] Castanier, M. P., and Pierre, C., 2006. "Modeling and Analysis of Mistuned Bladed Disk Vibration: Current Status and Emerging Directions". *Journal of Propulsion and Power*, **22**(2), pp. 384–396.
- [13] Kielb, R. E., Hall, K. C., Hong, E., and Pai, S. S., 2006. "Probabilistic Flutter Analysis of a Mistuned Bladed Disks". ASME Paper No. GT2006-90847.
- [14] Mayorca, M. A., Vogt, D. M., Mårtensson, H., and Fransson, T. H., 2010. "A New Reduced Order Modeling for Stability and Forced Response Analysis of Aero-Coupled Blades Considering Various Mode Families". ASME Paper No. GT2010-22745.
- [15] Martel, C., Corral, R., and Llorens, J. M., 2008. "Stability Increase of Aerodynamically Unstable Rotors Using Intentional Mistuning". *Journal of Turbomachinery*, **130**(1), pp. 011006.
- [16] Groth, P., Mårtensson, H., and Edin, N., 2010. "Exper-

- imental and Computational Fluid Dynamics Based Determination of Flutter Limits in Supersonic Space Turbines”. *Journal of Turbomachinery*, **132**(1), pp. 011010.
- [17] Groth, P., Mårtensson, H., and Andersson, C., 2010. “Design and Experimental Verification of Mistuning of a Supersonic Turbine Blisk”. *Journal of Turbomachinery*, **132**(1), pp. 011012.
- [18] Armstrong, E. K., and Stevenson, R. E., 1960. “Some Practical Aspects of Compressor Blade Vibration”. *Journal of the Royal Aeronautical Society*, **64**, pp. 117–130.
- [19] Baldwin, B. S., and Lomax, H., 1978. “Thin Layer Approximation and Algebraic Model for Separated Turbulent Flows”. AIAA Paper No. 78-0257.
- [20] Ning, W., and He, L., 1998. “Computation of Unsteady Flows Around Oscillating Blades Using Linear and Nonlinear Harmonic Euler Methods”. *Journal of Turbomachinery*, **120**(3), pp. 508–514.
- [21] He, L., 2000. “Three-Dimensional Unsteady Navier-Stokes Analysis of Stator-Rotor Interaction in Axial-Flow Turbines”. *Journal Proceedings of the Institution of Mechanical Engineers, Part A: Journal of Power and Energy*, **214**(1), pp. 13–22.
- [22] Chen, T., Vasanthakumar, P., and He, L., 2001. “Analysis of Unsteady Bladerow Interaction Using Nonlinear Harmonic Approach”. *Journal of Power and Propulsion*, **17**(3), pp. 651–658.
- [23] Sun, J., and Kari, L., 2010. “Coating Methods to Increase Material Damping of Compressor Blades: Measurements and Modeling”. ASME Paper No. GT2010-44014.
- [24] Vogt, D., 2005. “Experimental Investigation of Three-Dimensional Mechanism in Low-Pressure Turbine Flutter”. PhD Thesis, Royal Institute of Technology (KTH), Stockholm, Sweden.
- [25] Bladh, R., Castanier, M. P., and Pierre, C., 2001. “Component-Mode-Based Reduced Order Modeling Techniques for Mistuned Bladed Disks—Part I: Theoretical Models”. *Journal of Engineering for Gas Turbines and Power*, **123**(1), pp. 89–99.
- [26] Guyan, R., 1965. “Reduction of Stiffness and Mass Matrices”. *AIAA Journal*, **3**(2), p. 380.
- [27] Allemang, R. J., and Brown, D. L., 1982. “A Correlation Coefficient for Modal Vector Analysis”. In *Proc. 1st International Modal Analysis Conference*, Union College, Schenectady, NY, pp. 110–116.
- [28] Castanier, M. P., and Pierre, C., 2002. “Using Intentional Mistuning in the Design of Turbomachinery Rotors”. *AIAA Journal*, **40**(10), pp. 2077–2086.
- [29] Castanier, M. P., and Pierre, C., 1997. “Consideration on the Benefits of Intentional Blade Mistuning for the Forced Response of Turbomachinery Rotors”. In *Proceedings of the 1997 ASME International Mechanical Engineering Congress and Exposition*, Dallas, Texas, **55**, pp. 419–425.